Indian J. Phys. **77B** (1), 101-111 (2003)

AN INTERNATIONAL JOURNAL
IJP B

Impulsive stimulated Raman scattering by phonon polaritons and the Cherenkov effect

J K Wahlstrand* and R Merlin

Department of Physics, The University of Michigan, Ann Arbor, MI 48109-1120

e-mail : wahlstrj@umich.edu

Abstract Spatially resolved electro-optic sampling experiments on ZnTe and GaP demonstrate that the generation of coherent phonon polaritons by ultrafast optical pulses can be described as Cherenkov radiation. Coherent phonon polaritons generated through impulsive stimulated Raman scattering are usually studied using the transient grating geometry, in which two ultrafast pulses define a specific polariton wavevector. Alternatively, polariton generation using a tightly focused pump pulse is usually associated with the Cherenkov effect. Here we show that the two methods, stimulated Raman scattering and the Cherenkov interpretation, are fundamentally the same and discuss the implications of this on the interpretation of transient grating experiments. We also show that the generation of THz radiation by non-resonant optical rectification can be described as Cherenkov emission by a spatially extended source. Experiments and calculations are presented for various excitation geometries.

Keywords Impulsive stimulated Raman scattering, phonon polariton, Cherenkov radiation

PACS Nos. 71.36.+c 78.47.+p

1. Introduction

The names of two great experimental physicists are associated with the Raman effect and Cherenkov radiation (CR)[1, 2]. To the modern experimentalist, the methods by which they were discovered seem amazingly primitive and yet refreshingly simple. The Raman effect was discovered by focusing filtered sunlight into liquids and observing the inelastically scattered light through colored filters and polarizers,[1, 3] whereas CR was discovered when Cherenkov noticed a bluish glow in a crucible of sulfuric acid placed next to a piece of radium [2, 4]. There are some striking parallels between the early histories of these two phenomena. In both experiments,the photodetector was the human eye, the most sensitive real-time detector of visible light available at the time. In addition, much as in the case of Raman's early experiments, most of Cherenkov's early efforts went into proving that the light resulted from something other than simple luminescence, and he succeeded by demonstrating the radiation's strong forward collimation and polarization properties[4]

This paper deals with a phenomenon that is a combination of the Raman and Cherenkov effects. It is well-known in the ultrafast optics community that tightly focused optical pulses traveling through anonlinear medium can emit Cherenkov radiation [5, 6]. Through the inverse electro-optic effect, also known as optical rectification, such a pulse imitates a relativistic dipole. In a medium with dispersion, the Cherenkov radiation takes the form of a polariton, and the generation mechanism is a combination of both stimulated Raman and inverse electro-optic contributions. The Cherenkov formalism is useful for describing the effects of a source of polaritons propagating through a transparent material.[7, 8]

Stimulated Raman scattering is the coherent process in which two optical waves interact to generate or gain energy from a coherent phonon field. Impulsive stimulated Raman scattering (ISRS) describes the special case in which both optical waves are present in a single broadband pulse.[9] In the time domain,this is equivalent to the optical pulse producing a force on the lattice and starting a coherent phonon oscillation, which may then be detected with another pulse through the inverse process. Pump and probe measurements with ultrafast optical pulses have been used to generate and detect coherent and squeezed optical phonon fields in a variety of materials [10, 11]. Potential applications include an X-ray Bragg switch [12] and ferroelectric memory [13].

*Corresponding Author

Visible optical pulses can generate infrared light through difference-frequency generation (DFG), also known as optical rectification [14], associated with the nonlinear susceptibility $\chi^{(2)}$. The optical pulse is rectified, inducing a polarization proportional to its intensity envelope which then radiates infrared light. If the pulse is tightly focused and its group velocity is greater than the phase velocity in the infrared, the situation is analogous to CR, in that we have a relativistic object (a dipole) emitting light. This was first shown in 1984 by Auston and co-workers in $LiTaO_3$ [5] and was developed into a source of short THz pulses [15].

The connection between stimulated Raman scattering and the Cherenkov effect comes about because an infrared-active phonon couples strongly to light, resulting in a phonon polariton. Polaritons, hybrid excitations that result when an elementary excitation carries a polarization [16, 17], are, in some sense, a way of describing light propagation without introducing the index of refraction; the polariton is dressed light. Phonon polaritons were first studied experimentally by spontaneous Raman scattering in the near-forward scattering geometry [18]. Because of the coupling between the lattice and infrared light, a force on the lattice induced by the optical pulse results in infrared emission. As a result, stimulated Raman scattering and the electro-optic effect are mixed. Because a phonon polariton has a sizable group velocity, it propagates away as it is generated, and this is nicely taken into account by the Cherenkov formalism.

Recently, a pump-probe experiment in ZnSe led to a re-examination of electro-optic CR in dispersive media [7]. The fact that infrared light is a polariton results in strong dispersion near the phonon frequency, which changes the CR pattern. There are two qualitatively different regimes for CR depending on the velocity of the source, which were termed superluminal and subluminal. The subluminal regime contains features not previously recognized [19]. Recently, results of a spatially-resolved electro-optic sampling experiment in ZnTe were reported, in which the Cherenkov pattern in the subluminal regime was first measured [8]. In the ISRS literature, it is not commonly appreciated that ISRS and the Cherenkov effect are two sides of the same coin. The generation mechanism is identical, the only difference is the shape of the pump pulse, periodic for ISRS and point-like for the Cherenkov effect. ISRS is often discussed in terms of four-wave mixing, but the CR interpretation is, in our opinion, more physically revealing.

We performed experiments in two crystals, ZnTe and GaP. Our technique, based on that of Auston and co-workers [6], allows the detailed mapping of the polariton field generated by a pulse of any spatial or temporal shape, and at the same time images the source pulse itself. Our calculations, based on the Cherenkov radiation interpretation, could find application in the determination of the DFG-generated electromagnetic fields due to spatiotemporally-shaped ultrafast pulses [20].

2. Phonon polaritons and the optical susceptibilities

There are two equivalent ways of looking at phonon polaritons, as lattice vibrations coupled to the electromagnetic field, or as light perturbed by coupling to the lattice, leading to strong dispersion in the dielectric susceptibility. The important point is that the lattice and electromagnetic field cannot be separated, so interactions which affect the lattice necessarily couple to the electric field and vice versa. Here we review the optical phonon's contribution to the linear and nonlinear susceptibilities of the medium.

For simplicity, consider a single infrared-active mode in a diatomic lattice with cubic structure, and neglect damping. The dielectric function is [17]

$$\varepsilon(\Omega) = \varepsilon_\infty + \frac{\varepsilon_0 - \varepsilon_\infty}{1 - (\Omega / \Omega_{TO})}$$

where Ω_{TO} is the transverse optical phonon frequency, ε_∞ is the dielectric constant due to higher-lying electronic resonances, and ε_0 is the static dielectric constant. The coupling between the lattice and light leads to the breaking of the degeneracy between the longitudinal and transverse optical phonon frequencies Ω_{LO} and Ω_{TO}, which are related by the well-known Lyddane-Sachs-Teller formula $\Omega_{LO}^2 = \frac{\varepsilon_0}{\varepsilon_\infty} \Omega_{TO}^2$. The refractive index $n(\Omega) = \varepsilon(\Omega)^{1/2}$, phase velocity $c / n(\Omega)$, and polariton dispersion relation $\Omega = cq / n(\Omega)$ are shown in Figure 1 for a material with dielectric function given by Eq. 1. In this work we deal with the lower polariton branch, consisting of frequencies below Ω_{TO}. Near zero frequency where the dispersion curve is

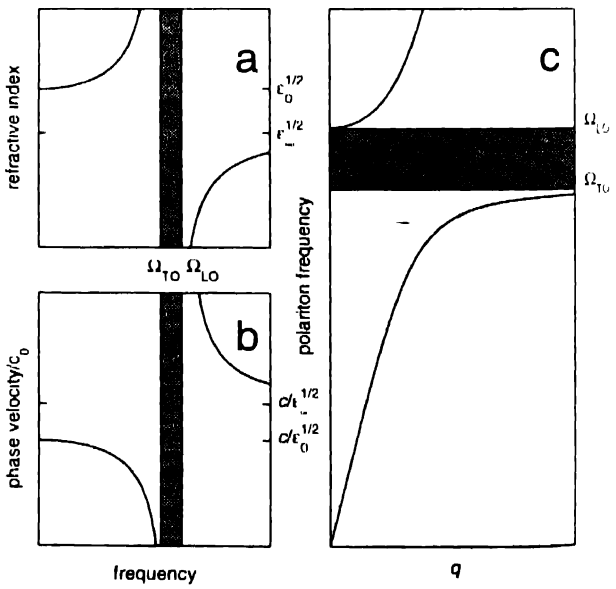

Figure 1. Optical parameters given by Eq. 1 for a generic material with a single infrared-active phonon. (a) Refractive index n. (b) phase velocity c/n. (c) polariton dispersion relation. The darkened regions indicate the band between Ω_{TO} and Ω_{LO} in which light cannot propagate.

linear, the polariton is mostly light-like whereas, near Ω_{TO}, it is phonon-like. In general, the polariton has both light-and phonon-like character.

Nonlinear interaction of visible light with phonon polaritons involves both the lattice and the THz electromagnetic field. The nonlinear tensor that determines the coupling of polaritons to visible light is thus composed of two parts, the Raman tensor $\frac{d\chi}{dQ} = \chi^R$, which couples visible light to the phonon mode with amplitude Q, and the second-order nonlinear susceptibility $\frac{dy}{dI} = \chi^{(2)}$, which couples visible light to electric fields. Both of these susceptibilities are almost entirely electronic in nature and, in the transparent materials discussed here, real. Counting both of these contributions, the total nonlinear polarization is [21, 17]

$$P_i^{NL}(\Omega) = \chi^{(2)}_{ijk} E_j(\Omega)\, E_k(\omega_L) + \chi^R_{ik}\, Q_j\, E_k(\omega_L), \quad (2)$$

where Q_j is the amplitude of one of the three-fold degenerate phonon modes, ω_L is the frequency of the visible laser light and Ω is the frequency of the phonon polariton. As is well-known, the Raman contribution can be included in an effective nonlinear susceptibility d_{ijk}, each tensor element of which takes the form

$$d(\Omega) = \chi^{(2)}\left[1 + C\left|1 - \frac{\Omega^2}{\Omega_{TO}^2}\right|^{-1}\right] \quad (3)$$

where the Faust-Henry coefficient $C = \chi^R\left(\chi^{(2)}\right)^{-1} e^* \mu^{-1} (\Omega_{TO})^{-2}$ gives the ratio of the Raman (often termed ionic) to electronic contributions [21]. Here e^* is the transverse effective charge and μ is the reduced mass of the lattice mode. Because

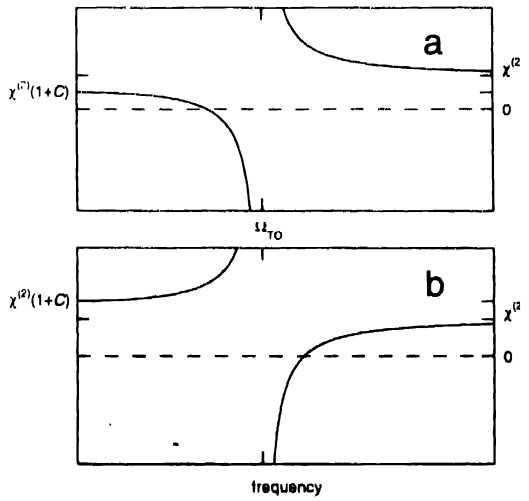

Figure 2. Effective nonlinear susceptibility $d(\Omega)$ according to Eq 3 (a) $C = -0.5$ The $\chi^{(2)}$ and Raman contributions subtract below the resonance.(b) $C = 0.5$ The $\chi^{(2)}$ and Raman contributions add below the resonance

χ^R and $\chi^{(2)}$ do not change appreciably with frequency in the THz range, C is nearly a constant for a given laser wavelength and material. See Figure 2. In our experiments we shall not need to consider the dispersion of d, for we mainly deal with low frequency polaritons. We assume a constant nonlinear susceptibility given by $\chi^{(2)}(1+C)$.

3. Theory of Cherenkov radiation in a dispersive medium

After including the Raman contribution to the generation and detection of polaritons in an effective electro-optic coefficient $d(\Omega)$, we can now use the theory of Cherenkov radiation to calculate the polariton field. The theory of CR by a charged particle was largely worked out by Tamm and Frank in the late 1930's [22, 23] and adapted to electro-optic CR by Kleinman and Auston in 1984 [24]. A charged particle that travels through a dielectric kicks the electrons in the medium, and when the particle travels faster than the phase velocity of light in the medium, an electromagnetic shock wave is generated, analogous to a sonic boom. This is Cherenkov radiation.For wavelengths much larger than the lattice spacing, the theory of CR is entirely classical and derivable with the macroscopic Maxwell equations.

Within the slowly-varying envelope approximation, an optical pulse traveling through a non-centrosymmetric medium mixes with itself and induces a polarization proportional to its pulse envelope [14]. This dipolar charge distribution moves at the group velocity v_g of the pulse and, like a charged particle, can emit CR if v_g is greater than the phase velocity of light $c/n(\Omega)$ within the bandwidth of the rectified pulse. Note that the CR interpretation of this process is still that of a nonlinear optical process; DFG induces the relativistic dipole and the Cherenkov formalism is simply another way of describing the phase matching process. It is also possible in some situations to interpret other nonlinear optical phase matching processes, like second harmonic generation, in Cherenkov-like terms [25].

If the beam is focused tightly compared to the wavelength of the polariton, the polarization induced by the ultrafast optical pulse can be approximated by a point dipole. This is the closest optical analogue to conventional CR (emitted by a relativistic monopole). We assume that the optical pulse is never depleted by the DFG process and make the approximation that the medium is infinitely long, so that, if the source of CR travels along the z axis, the fields are a function of $z - v_g t$ and the cylindrical coordinates ρ, measured from the pulse's path through the sample and ϕ, measured from the direction of the dipole.

The CR electric field of a dipole is proportional to the derivative of the point charge field along the direction of the dipole orientation [4]. For a dipole oriented perpendicular to the z axis,the field is proportional to $\cos\phi$. For simplicity we drop the ϕ dependence in the following,and obtain

$$E_z(\rho, z - v_g t) \propto \int_{-\infty}^{\infty} \frac{ic}{v_g^2 n^2(\Omega)} \frac{\partial a}{\partial \rho} \Omega d\Omega \quad (4)$$

$$E_\rho(\rho, z - v_g t) \propto \int_{-\infty}^{\infty} e^{i\Omega[\,\cdot\,]} \frac{\partial^2 a}{n^2(\Omega)\,\partial \rho^2} d\Omega, \quad (5)$$

where E_z and $H_0^{(2)}$ are the z and ρ components of the electric field, respectively, and

$$a(\rho, \Omega) = -iH_0^{(2)}[s(\Omega)\rho] \text{ if } \Omega > 0$$

$$a(\rho, \Omega) = iH_0^{(1)}[s(\Omega)\rho] \text{ if } \Omega < 0 \quad (6)$$

where $H_0^{(1)}$ and $H_0^{(2)}$ are Hankel functions and $s(\Omega) = \Omega(\varepsilon v_g^2/c^2 - 1)^{1/2}/v_g = \Omega \tan\theta_c / v_g$ [4].

Because we are interested in the far field radiation, we restrict the integral to the range for which the Cherenkov condition is satisfied $v_g > c/n(\Omega)$. If $v_g > c/n(0)$, the laser pulse travels faster than the entire lower polariton branch, so we integrate over $0 < \Omega < \Omega_{1Q}$. This is what we call the superluminal regime. If instead $v_g < c/n(0)$, the laser pulse only travels faster than frequencies in the range $\Omega_c < \Omega < \Omega_{1Q}$, where Ω_c is defined by $v_g = c/n(\Omega_c)$. We refer to this as the subluminal regime. While this terminology has been brought into question recently by Ginzburg [26] we feel that it provides a sharp distinction between these two qualitatively very different regimes.

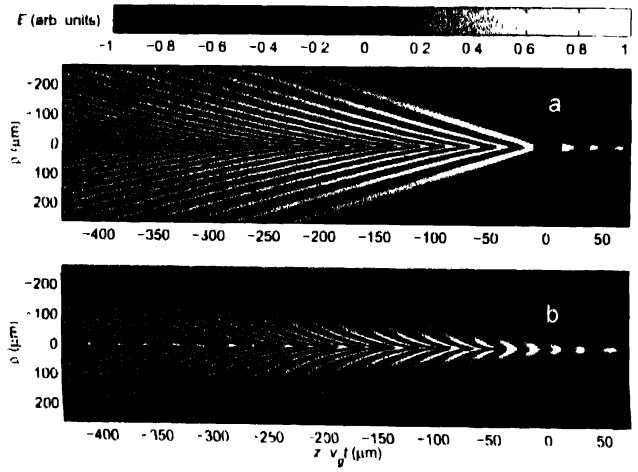

Figure 3. Calculation of E_ρ, plotted according to the color scale shown, due to a point dipole located at $\rho = 0$ and $z - v_g t = 0$ traveling to the right at speed v_g through a medium with dispersion given by Eq.1 (a) Superluminal regime ($v_g > c/n(0)$) (b) Subluminal regime ($v_g < c/n(0)$)

Plots of E_ρ calculated using Eq 5 in a medium with $n(\Omega)$ given by eq. (1) are shown in Figure 3 In the superluminal regime (Figure 3a), there is a sharp shock front and the effect of the dispersion is to add ripples behind it, as shown in the original experiment in $LiTaO_3$, [5] a material which is firmly in the superluminal regime due to its large ε_0. The subluminal regime (Figure 3b) is qualitatively very different. The phase front angle is dependent on ρ, and there is also a large field near $\rho = 0$ As in the superluminal regime, the radiation pattern is confined within a cone, but the cone angle becomes larger as v_g decreases, in contrast with the superluminal case. These features are apparent in the calculations reported by Afanasiev *et al* [19].

Physical understanding of the differences between the two regimes can be extracted from an approximate analytical treatment in the limit of large ρ. Taking E_ρ as an example and using the large argument asymptotic form of the Hankel function, Eq. 5 becomes

$$E_\rho \propto \int_{\Omega_c}^{\Omega_{1Q}} \frac{i\sqrt{2s^3(\Omega)}}{n^2(\Omega)\sqrt{\pi\rho}} e^{-i[\Omega(t - z/v_g) - s(\Omega)\rho + \pi/4]} d\Omega. \quad (7)$$

For large ρ, this integral is large only where the integrand does not oscillate, so by the stationary phase method, it may be approximated as

$$E_\rho \propto \sum_{\Omega_i} \frac{2\sqrt{s^3(\Omega_i)}}{n^2(\Omega_i)\rho} \frac{1}{|s''(\Omega)|} e^{-i[\Omega_i(t - z/v_g) - s(\Omega_i)\rho]}, \quad (8)$$

where Ω_i are the frequencies within the range of integration for which the phase in the exponential is stationary. These are the solutions to

$$v_g \frac{ds}{d\Omega} = \frac{v_g t - z}{\rho} = \cos\theta, \quad (9)$$

which defines a cone of angle θ to the z axis.

The cone angle depends on frequency because $s(\Omega)$ contains $n(\Omega)$ Eq.9 becomes

$$v_g \frac{ds}{d\Omega} = \Omega^2 \frac{v_g}{sc^2} \frac{d\varepsilon}{d\Omega} + \frac{v_g s}{\Omega} = \cot\theta. \quad (10)$$

The dependence of θ on Ω is plotted for the two regimes in Figure 4. In the superluminal regime, θ is a monotonic function of frequency, whereas in the subluminal regime two frequencies map onto the same angle, resulting in the complex beating behavior shown in Figure 3b.

The angle θ_C, defined as the smallest angle at which radiation is emitted, is shown as a dashed line in Figure 4. The frequency that gives this confining angle is a solution to $s''(\Omega) = 0$. In the superluminal regime, $\varepsilon(\Omega)v_g^2/c^2 - 1 > 0$ for all frequencies within the range of integration, and $\Omega = 0$ is the

only solution. From Eq. 10, we then get $\cos\theta_C = v_g n(0)/c$, the standard Cherenkov expression. In the subluminal regime, there are two solutions. For a material with dispersion given by Eq.1

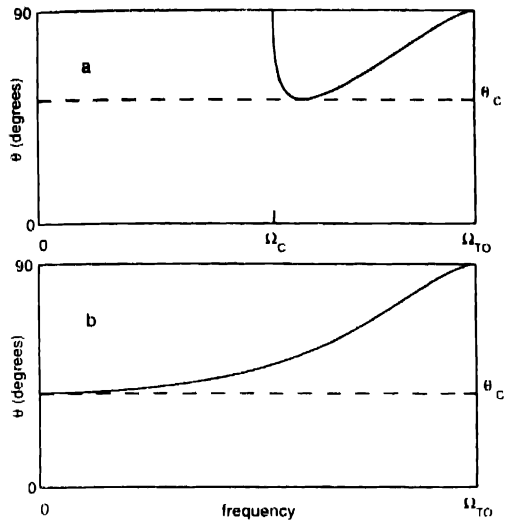

Figure 4. Plot of Eq. 10 for various source velocities. The dashed line indicates the Cherenkov angle θ_C and Ω_C indicates the group velocity matched frequency in the subluminal regime (a) Subluminal regime (b) Superluminal regime

$\theta_C = \tan^{-1}(4\gamma^{-1}\sqrt{(\eta-\zeta)/\zeta^3})$, where $\gamma = (1-\varepsilon_\infty v_g^2/c^2)^{-1/2}$ and $\eta = 1-(\Omega_C/\Omega_{TO})^2$ [19]

The point dipole solution is useful as a test case, but difficult to approach experimentally due to the tight focus needed. Before turning to a general case, we focus on the somehow opposite limiting case, when the beam waist w is much larger than the wavelength of the polariton ($w >> 2\pi c/\Omega$). Here the Cherenkov source is a wall of dipoles traveling through the medium at the group velocity of the pulse.Because the pump pulse contains wavevectors pointing only in the direction of propagation, we expect polaritons to be emitted exclusively in the forward direction.

For an infinitely thick crystal, the source polarization is $P = \zeta\delta(z-v_g t)e_d$, where e_d is a unit vector pointing inthe direction of the dipole and ζ is the areal polarization. It is possible to obtain the CR field from the point dipole solution by convolution, but here we use the method of Kleinman and Auston and calculate the Hertz potential [24]

$$\Pi(\Omega) = -\frac{4\pi\zeta e^{-i\Omega(t-z/v_\varphi)}}{v_\varphi \varepsilon(\Omega) s^2(\Omega)} \tag{11}$$

The electric field from this potential is [7]

$$E = \int_0^{\Omega_{LO}} \frac{\varepsilon(\Omega)\Omega^2}{c^2}\Pi(\Omega)d\Omega \tag{12}$$

$$= -\frac{4\pi\zeta}{v_g c^2} e_d \int_0^{\Omega_{LO}} \frac{\Omega^2 e^{-i\Omega(t-z/v_\varphi)}}{s^2(\Omega)} d\Omega. \tag{13}$$

In the superluminal regime, $s^2(\Omega) > 0$, and the integral vanishes. We get a non-zero result when $s^2(\Omega) = 0$, which only occurs in the subluminal regime at Ω_C, the polariton frequency velocity-matched to the pulse. We emphasize that the phase matching condition is only met in the presence of dispersion. In the superluminal regime, no radiation is emitted from the bulk because the pulse is traveling faster than all of the infrared frequencies generated.

Practically, a beam cannot be focused to a point, nor is it really planar. Any real source behaves as apoint for long wavelength polaritons and as a plane for short wavelength polaritons. We compare experiments with calculations by convoluting the point solution with the pulse envelope. Calculations for extended sources are shown in Figure 5.

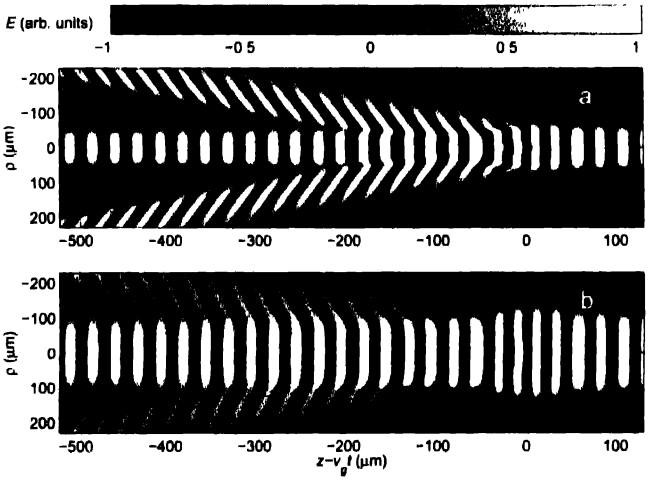

Figure 5. Calculation of E_ρ in the subluminal regime for an extended source of width w obtained by convoluting the point calculation with a Gaussian in the ρ direction (a) w = 20 μm (b) w = 40 μm

4. Materials

The generation of electro-optic CR requires a non-zero $\chi^{(2)}$ present only in crystals without inversion symmetry. In our experiments, we used ZnTe and GaP, readily available and well-characterized materials. See Table 1 for the parameters relevant to this work.

Materials with the zinc blende structure have a triply degenerate infrared-active optical phonon mode. For light normally incident on a (110) oriented crystal, the selection rules forbid excitation of the LO mode. For the doubly degenerate TO mode,

$$R_1 = \begin{pmatrix} 0 & 0 & -b \\ 0 & 0 & b \\ -b & b & 0 \end{pmatrix} \quad \text{and} \quad R_2 = \begin{pmatrix} 0 & b & 0 \\ b & 0 & b \\ 0 & 0 & 0 \end{pmatrix} \tag{14}$$

Table 1. Table of parameters used in the calculations for the zinc blende materials studied here. The group velocity matched frequency Ω_c was calculated using the listed n_g and $n(\Omega)$.

Parameter	GaP	ZnTe	Units
$\Omega_{TO}/2\pi$	11.0 [27]	5.32 [28]	THz
$\Omega_{LO}/2\pi$	12.1 [27]	6.18 [28]	THz
$\sqrt{\varepsilon_0}$	3.31 [29]	3.16 [30]	
n_g at 800 nm	5.56 [29]	3.24 [31]	
$\Omega_c/2\pi$	7.7	2.1	THz

where R_1 and R_2 are the Raman tensors for the modes polarized along the $(1\bar{1}0)$ and (001) directions, respectively. The single independent tensor component b corresponds to the electro-optic coefficient d_{41}, with the effective electro-optic tensor $d(\Omega)$ given by eq. (3). The dipolar distribution induced by the pump pulse is oriented perpendicular to the (110) direction, the pulse's direction of motion. We measure the phonon polariton amplitude by the linear electro-optic effect. Because of symmetry, the probe pulse is only sensitive to the electric field component E_ρ perpendicular to the z axis.

Faust and Henry found, in their pioneering work using nonlinear mixing of visible and infrared cw laserlight, that $C = -0.47$ in GaP [21]. This leads to total destructive interference between the ionic and electronic contributions to d at 6.5 THz. Because this is close to Ω_c for Ti:sapphire pulses, the expected signal is small. Recently Leitenstorfer et al measured $C = -0.07$ in ZnTe by analyzing data from time-domain spectroscopy of THz pulses by electro-optic sampling [32]. This small value for C leads to $d = 0$ at 5.2 THz, very close to Ω_{TO}. For our experiment in ZnTe, we are only able to measure up to roughly 4 THz, not high enough to be sensitive to any effects of the dispersion of d.

5. Experiments

Our technique is based on that of Auston *et al* [5]. A diagram of the experimental setup is shown in Figure 6. Pulses from an ultrafast laser are split into pump and probe beams and focused to a common spot inside the sample. The pump pulse is the source of CR. The tightly focused probe pulse travels along behind the pump pulse and samples the field through the linear electro-optic effect, which causes a measurable change in the polarization of the probe pulse. When properly oriented, the polariton's electric field induces birefringence, which can be probed by measuring the polarization state of the probe after the sample. This yields a signal directly proportional to the THz Cherenkov electric field. By changing the time delay (t) between pump and probe with a motorized delay stage in the probe path, and the relative focal position (ρ) by moving the motorized translation stage upon which the pump lens is mounted, we map the polariton field in two dimensions, measuring the polarization of the probe pulse.

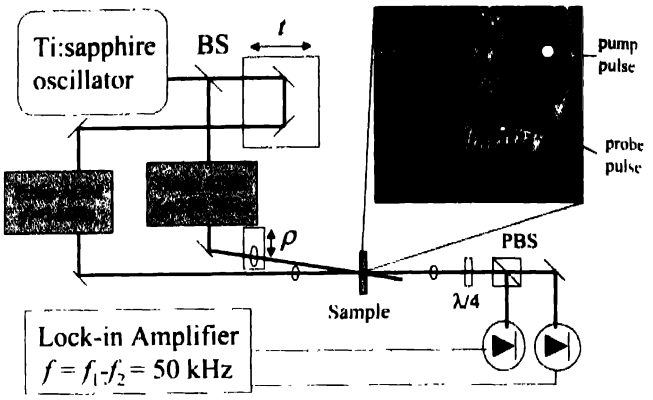

Figure 6. Experimental setup. Pulses are split into pump and probe paths, the time delay (t) between which is varied with an automated translation stage. The relative position (ρ) of the two beams is controlled by changing the position of the pump lens. The polarization of probe beam is detected with a polarizing beam splitter and two diodes, with the lock-in detecting the difference between the two signals. At top right is a close-up of the geometry inside the crystal. The pump and probe pulses travel along parallel paths inside the crystal at the same group velocity v_g.

Good spatial resolution requires that the two pulses propagate as collinearly as possible inside the sample, so the pump and probe beams are focused with two small lenses placed close together. In order to prevent walking of the pump and probe pulses spatially as they propagate through the crystal, we made the plane shared by the pump and probe beams perpendicular to the axis along which the pump lens is moved. We accomplished this by directing the probe beam below the pump lens, and the relative focal position was moved horizontally. Resolution in $z - vt$ is determined by the pulse width of the probe pulse and resolution in ρ by the focal waist of the probe beam. The convoluted spot size inside the crystal was measured using the same technique. In ZnTe and GaP, two photon absorption depletes the probe when pump and probe overlap temporally and spatially, creating a large Gaussian peak.

The source of ultrafast pulses was a Ti:sapphire oscillator producing 60 fs pulses with central wavelength 800 nm at repetition rate 82 MHz. Acousto-optic amplitude modulators were used to modulate the pump and probe beams at 3 MHz and 2.95 MHz, respectively, and the probe was detected with a lock-in amplifier at the difference frequency 50 kHz. The maximum pump and probe average powers at the sample were roughly 140 and 30 mW, respectively, limited mainly by the efficiency of the modulators. We emphasize the importance of the double-modulation technique because it rejects scattered pump light. Recently, similar experiments have been performed using the Zernike phase contrast method with a CCD camera, to image the phase change of a weakly-focused probe beam caused by the polariton as a function of position and time delay [33, 34]. These measurements are basically equivalent to our experiments.

To attain the point dipole geometry, the pump pulse must be focused to a spot smaller than the wavelength of the polariton. Because we use thick crystals, we are limited to a focal waist of about 20 μm which, depending on the material, corresponds to a maximum polariton frequency of 2-4 THz.

Results of our experiment and calculations in ZnTe, a subluminal material, are shown in Figure 7. The (110) oriented sample was 1 cm^2 by 1 mm thick. The data clearly shows many of the features predicted for subluminal CR. The artifact that appears about 1.6 ps after the pump pulse isdue to a second pulse about 1000 times smaller than the pump pulse, which is probably due to a reflection from an optical element upstream. There is another signal, an exponential decay behind the pump pulse due to the change in refractive index caused by free carriers generated by two-photon absorption. This signal is partially balanced out by using polarization-sensitive detection, and the remnant has been fitted and subtracted out in Figure 7a.

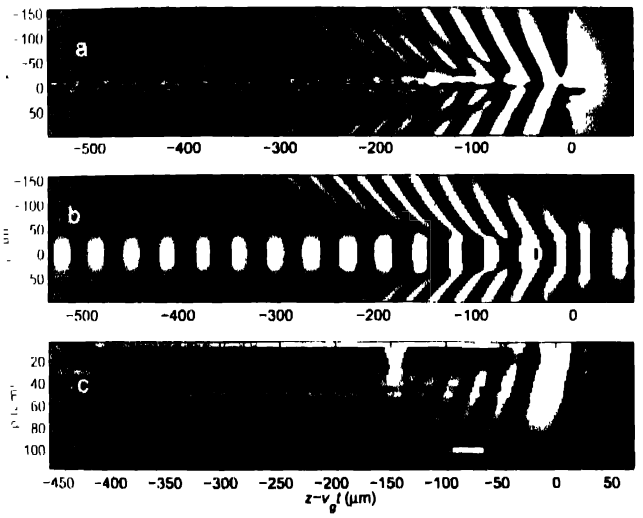

Figure 7. (a) Results of a pump-probe differential transmission experiment in ZnTe. An overall constant background was subtracted for each time scan and a decaying exponential was subtracted out for the time scans near $\rho = 0$. The feature 1.6 ps behind the pump pulse is an artifact due to an extra pulse. (b) Calculation with a point dipole convoluted with a 22 μm Gaussian in the transverse direction. (c) Results of a pump-probe experiment in a 300 μm thick ZnTe sample.

As discussed earlier, the CR field in the subluminal regime can exhibit a beating pattern. There is a striking node, shown in Figure 7a that separates the shock wave into two or three distinct parts. This node can be explained by both subluminal beats and a convolution artifact due to the finite spatial size of the pump and probe pulses, but is not as clear in the calculation. This discrepancy, plus the lack of signal near $\rho = 0$ in the experiment is probably due to the finite size of the crystal, as discussed in detail later.

Results for the planar geometry in GaP and ZnTe with a pump waist of roughly 100 μm are shown in Figure 8. The GaP sample was a 4 by 1 by 1 mm crystal. The time scans show the group velocity matched frequencies predicted by v_g and $n(\Omega)$, with an apparent decay probably due to a combination of the finite length of the sample, as discussed later, and the finite extent of the pump pulse, as described in [7]. As discussed above, the planar geometry is that used for the generation of THz pulses by nonresonant optical rectification [35]. The dependence of the distortion of a transmitted THz pulse on crystal thickness and laser wavelength has received a lot of attention recently [36, 37], and our experiment and calculations are relevant to that problem.

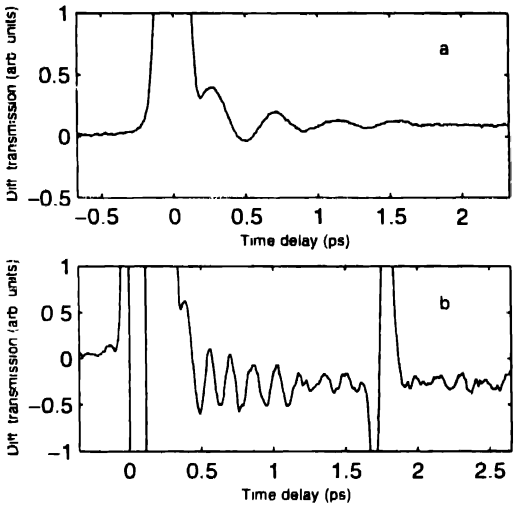

Figure 8. Results of a pump-probe experiment with weakly focused ultrafast pulses in ZnTe and GaP.The region near time zero is dominated by two-photon absorption (a) 1 mm thick ZnTe crystal. The main frequency is roughly 2 THz (b) 1 mm thick GaP crystal. The main frequency is roughly 7.5 THz. The feature at 1.7 ps is an artifact due to a second pulse.

Experiments using the point geometry were also performed on a 300 μm thick ZnTe sample, where, as is apparent in Figure 7c, the node disappears. We believe this is a result of the breakdown of the infinite crystal approximation. In the superluminal regime, the infinite crystal calculation works quite well, because the polaritons generated by the pulse are emitted at a large angle at all frequencies down to zero. Therefore effects of the finiteness of the crystal can be expected at the very edge of the shock wave, at $\rho = L \tan \theta_C = Ln_0 / c$, where L is the length of the crystal.

In the subluminal regime, polaritons near Ω_C are sent in a near forward direction, and this complicates matters. For example, in our 1 mm thick ZnTe crystal, the Cherenkov angle of 2.5 THz polaritons is about 9 deg, so that component only reaches ρ = 160 μm before the pulse arrives at the end of the crystal. In a 300 μm thick crystal, it only reaches ρ = 50 μm. The subluminal beats, due to interference between frequency components sent in the forward direction, require some propagation time to develop and this might be the reason why they do not appear in a thin crystal, as is evident in Figure 7c.

These arguments could also explain some other discrepancies between calculations and experiments in Figure

7. The large oscillatory signal at Ω_{ℓ} near $\rho = 0$ in the calculation is clearly absent in the experimental data, probably because Ω_{ℓ} is sent in the forward direction, and thus the finiteness of the crystal plays a large role. The difference in the shape of the cone between theory and experiment could be due to the same effect. A finite crystal calculation is probably needed in order to fully understand the details of the subluminal experiment. Note that calculation of CR in a finite crystal is similar to the so-called "Tamm problem" of CR from a particle traveling along a finite path [23, 38].

The finiteness of the crystal can be expected to play an even more important role in the planar geometry, in which Cherenkov components are emitted exclusively in the forward direction. The CR pattern is the result of interference among these components, so this pattern should change dramatically with crystal thickness. A very thin crystal would show no propagation effects, simply reproducing the time derivative of the pump pulse envelope as a short THz pulse. A thick crystal should approach the infinite limit discussed here.

6. Transient grating and phase matching issues

The most common approach used to excite and detect coherent polaritons is by using the transient grating technique [39, 40, 41], in which two pump pulses interfere inside the crystal, setting up an intensity grating which generates a coherent polariton field with a well-defined wavevector (and therefore frequency). This mechanism is identical to that of the Cherenkov radiation experiment, the only difference being the shape of the source, which is now periodic. We can calculate the polariton field generated by such a source using the machinery described above. If we cross two pump beams of equal intensity at an angle β, Gaussian in space with waist w inside the sample and Gaussian in time with pulsewidth τ, the intensity grating has the form

$$I(x, y, z - v_g t) \propto e^{-(x^2+y^2)/w^2} \cos\left(\frac{k_l x}{\sin\beta}\right) e^{-(z/v_g - t)^2/\tau^2} \qquad (15)$$

where k_l is the wavevector of the laser light inside the medium. Here we have assumed that β is small, which makes v_g equal to the group velocity of each separate pulse. This is a good approximation for the experiments described here, since k_l is much larger than the wavevector of the gratings. The Cherenkov angle converts the spatial periodicity of the transient grating into a temporal periodicity in the polariton field, resulting in a checkerboard pattern and a well-defined polariton frequency Ω; (see Figure 9)

Note that the wavevector of the grating is not the same as the polariton wavevector, since the polariton propagates in the direction normal to the wavefront. The magnitude of the polariton wavevector is $q = k_l \sin\theta$, where θ is the Cherenkov angle. In many older ISRS papers, it is assumed that the wavevector of the grating is the same as the polariton wavevector, which only applies to situations when θ is very large. This is generally a poor approximation, and, as recently pointed out by Hebling, leads to incorrect polariton dispersion measurements [42].

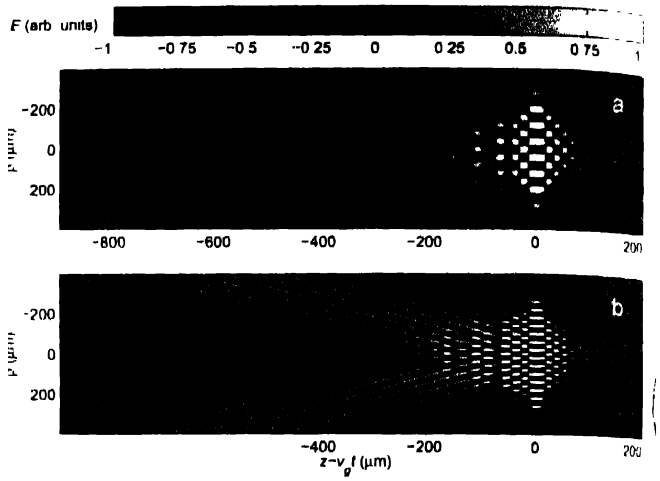

Figure 9. Calculation of E_p due to a transient grating, showing the checkerboard polariton field pattern generated behind the grating for two different grating periods.

The simple interpretation above works best for large w, in which case the polariton wavevector is well-defined. For small w, edge effects make the polariton field more complex, but by convoluting the point dipole solution with the grating, as shown in Figure 9, we can calculate what the polariton field would be due to gratings of arbitrary shape. This provides a potentially powerful machinery for calculating the polariton field generated by ultrafast optical pulses which have been shaped spatially and temporally, for example, in the manner recently suggested by Koehl *et al.*[33] To the best of our knowledge, this approach has not yet been applied to this problem.

It is useful to relate the Cherenkov interpretation to phase matching arguments. An ultrafast pulse contains a continuum of frequencies and wavevectors, and whether by ISRS or DFG, polariton generation obeys phase matching. The Cherenkov interpretation is another way of expressing this. The polarization is proportional to terms like $e^{i(k_2 - k_1)z - i(\omega_2 - \omega_1)t}$, where k_1, k_1, ω_1, and ω_2 denote wavevector and frequency components of the optical pulse. For the case of a planar geometry, the wavevector components point along the z axis, and conservation of momentum requires $q = k_2 - k_1 = [\omega_2 n(\omega_2) - \omega_1 n(\omega_1)]/c$, where q is the polariton wavevector. Since $\Omega = \omega_1 - \omega_2$,

$$q = \frac{\omega_2 n(\omega_2) - (\omega_2 + \Omega) n(\omega_2 + \Omega)}{c}$$

$$\approx \frac{\Omega}{c}\left(n(\omega_2) + \omega_2 n'(\omega_2)\right) = \frac{\Omega}{v_g(\omega_2)}, \qquad (17)$$

making the connection to the group velocity matching argument derived above.

A tightly focused optical pulse has wavevector components pointing in many directions. The dependence of the polarization on $z - v_g t$ forces $q_z = \Omega / v_g$. The polariton wavevector and frequency must also satisfy $\Omega = |\boldsymbol{q}| c / n(\Omega)$. Let q_ρ be the component of the polariton wavevector perpendicular to the z axis. Momentum conservation gives

$$\frac{q_\rho}{q_z} = \frac{\sqrt{q^2 - q_z^2}}{\Omega / v_g} = \sqrt{\frac{n^2(\Omega) v_g^2}{c^2} - 1}\,, \tag{18}$$

and the polariton is emitted at an angle $\tan^{-1} q_\rho / q_z$ to the z axis, identical to the Cherenkov angle. In the transient grating geometry, $\boldsymbol{k}_1$ and $\boldsymbol{k}_2$ are well-defined, and the wavevector $\boldsymbol{q} = \boldsymbol{k}_1 - \boldsymbol{k}_2$ is emitted in the direction given by Eq.18 because the polarization is a function of $z - v_g t$. As is well-known, it is possible to interpret ISRS as four wave mixing [40]. Here one hides both the generation and detection of the polariton in $\chi^{(3)}$, much as we included the Raman contribution to the generation of the polariton in $\chi^{(2)}$. The four-wave mixing polarization is

$$P(\omega_s) = \chi^{(3)}_{eff}(\omega_p, \Omega - \omega_p, \omega_p) E_1(\omega_1)\, E_2^*(\omega_1 - \Omega) E_p(\omega_p) \tag{19}$$

$$= d(\Omega, \omega_p)\left[d(\omega_1, \Omega - \omega_1) E_1(\omega_1) E_2^*(\omega_1 - \Omega)\right] E_p(\omega_p) \tag{20}$$

where E_1 and E_2 are the pump fields and E_p is the probe field, and d is the effective nonlinear susceptibility defined in Section 3. All propagation and damping effects can be included $\chi^{(3)}_{eff}$, and this formalism is often used [43].

4. Conclusions

The analogy between ISRS generation of polaritons and Cherenkov radiation is a good example of the power of analogies between seemingly unrelated fields. The observation that DFG in a bulk transparent material can be related to the emission of radiation by relativistic charged particles is not all that surprising since it results from a polarization induced by a traveling optical pulse. This dipolar charge distribution moves along with the pulse, emitting radiation as it travels through the medium. There exists a large volume of theoretical work in the field of radiation by uniformly moving charges [4, 44], which includes CR and transition radiation, and there probably exist other fruitful analogies to nonlinear optical processes.

We would like to discuss the advantages and disadvantages of the various scattering geometries available for coherent generation and detection of polaritons; see Figure 10. The "Cherenkov" experiments in the superluminal regime, shown in Figure 10a, produce the highest peak polariton amplitudes, but a wide range of polariton wavevectors and frequencies. ISRS by a transient grating, shownin Figure 10b, has the advantage of defining the polariton wavevector and producing a large amplitude polariton in that wavevector. The planar geometry in the subluminal regime, shown in Figure 10c, produces a polariton frequency given by group velocity matching considerations.

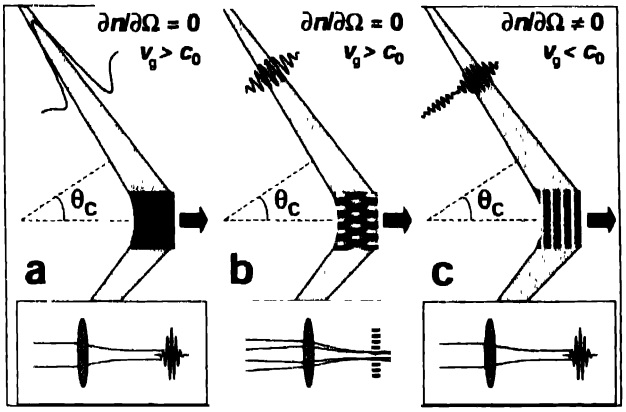

Figure 10. Various geometries for the generation of coherent polaritons, showing the near and far polariton fields generated (a) Single pump pulse in a superluminal material (b) Transient grating geometry (c) Single pump pulse in a subluminal material

In summary, we have experimentally imaged subluminal CR in ZnTe, verifying that CR takes the form of a cone even in the subluminal regime. We have shown that, in the planar regime, the response is dominated by the group velocity-matched polariton frequency Ω_C. We have shown that transient grating experiments can successfully be interpreted in terms of CR by a periodic dipolar distribution, and that phase matching arguments can be reconciled with the Cherenkov interpretation.

Thanks to G Narayanasamy for assistance with the experimental setup, to M DeCamp, C Herne, and J Murray for lending us ZnTe samples, and to T E Stevens and J Kuhl.

References

[1] C V Raman *A New Radiation Indian J. Phys.* **2** 387 (1928)

[2] P A Cherenkov *Doklady* AN SSSR **2** 451 (1934)

[3] G Venkataraman *Journey Into Light: Life and Science of C V. Raman, Indian Academy of Sciences* (1988)

[4] V P Zrelov *Cherenkov Radiation in High-energy physics, Israel Program for Scientific Translation* (1970)

[5] D H Auston, K P Cheung, J A Valdmanis and D A Kleinman, *Cherenkov Radiation from Femtosecond Optical Pulses in Electro-Optic Media, Phys. Rev Lett* **53** 1555 (1984)

[6] David H Auston and Martin C Nuss *Electrooptic Generation and Detection of Femtosecond Electrical Transients, IEEE J Quant. Electron.* **24** 184 (1988)

[7] T E Stevens, J K Wahlstrand, J Kuhl and R Merlin *Subluminal Cherenkov radiation: phonon-assisted phase matching, Science* **291** 626 (2001)

[8] J K Wahlstrand, T E Stevens, J Kuhl and R Merlin *Coherent polaritons and Cherenkov radiation Physica* B, **316-317** 55 (2002)

[9] Yong Xin Yan and Keith A Nelson *Impulsive stimulated light scattering. I. General theory*, *J. Chem. Phys.* **87** 6240 (1987)

[10] Lisa Dhar, John A. Rogers, and Keith A. Nelson *Time-Resolved Vibrational Spectroscopy in the Impulsive Limit*, *Chem. Rev.*, **94** 157 (1994)

[11] R. Merlin *Generating coherent THz phonons with light pulses*, *Solid State Commun.* **102** 207 (1997)

[12] P. H. Bucksbaum and R. Merlin *Solid State Commun.* **111** 535 (1999)

[13] S. Fahy and R. Merlin *Phys. Rev. Lett.* **73** 1122 (1994)

[14] M. Bass, P. A. Franken, J. F. Ward and G. Weinreich *Optical Rectification*, *Phys. Rev. Lett.*, **9** 446 (1962)

[15] B. B. Hu, X-C. Zhang, D. H. Auston and P. R. Smith *Free-space radiation from electro-optic crystals*, *Appl. Phys. Lett.* **56** 506 (1990)

[16] M. Born and K. Huang *Dynamical Theory of Crystal Lattices*, (Oxford : Oxford University Press) (1954)

[17] D. L. Mills and E. Burstein *Polaritons : the electromagnetic modes of media*, *Rep. Prog. Phys.* **37** 817 (1974)

[18] C. H. Henry and J. J. Hopfield *Phys. Rev. Lett.* **15** 964 (1965)

[19] G. N. Afanasiev, V. G. Kartavenko and E. N. Magar *Physica B*, **269** 95 (1999)

[20] Richard M. Koehl and Keith A. Nelson *Terahertz polaritonics : automated spatiotemporal control over propagating lattice waves*, *Chem. Phys.* **267** 151 (2001)

[21] W. L. Faust and Charles H. Henry *Mixing of visible and near resonance infrared light in GaP*, *Phys. Rev. Lett.* **17** 1265 (1966)

[22] I. Frank and I. Tamm *Dokl. Akad. Nauk. SSSR* **14** 109 (1937)

[23] I. Tamm *J. Phys.* **1** 439 (1939)

[24] D. A. Kleinman and D. H. Auston *Theory of Electrooptic Shock Radiation in Nonlinear Optical Media*, *IEEE J. Quantum Electron.* **20** 964 (1984)

[25] P. K. Tien, R. Ulrich and R. J. Martin *Optical second harmonic generation in form of coherent cherenkov radiation from a thin-film waveguide*, *Appl. Phys. Lett.*, **17** 447 (1970)

[26] V. L. Ginzburg *Physics-Uspekhi* **45** 341 (2002)

[27] A. Mooradian and G. B. Wright *Solid State Commun.* **4** 431 (1966)

[28] G. Gallot, Jianqquan Zhang, R. W. McGowan, Tae-In Jeon and D. Grischkowsky *Measurements of the THz absorption and dispersion of ZnTe and their relevance to the electro-optic detection of THz radiation*, *Appl. Phys. Lett.* **74** 3450 (1999)

[29] A. N. Pikhtin, V. T. Prokopenko and A. D. Yas'kov *Sov. Phys. Semicond.* **10** 1224 (1976)

[30] A. Manabe, A. Mitsuishi and H. Yoshinga *Jpn. J. Appl. Phys.* **6** 593 (1967)

[31] D. T. F. Marple *J. Appl. Phys.* **35** 539 (1964)

[32] A. Leitenstorfer, S. Hunsche, J. Shah, M. C. Nuss and W. H. Knox *Detectors and sources for ultrabroadband electro-optic sampling : Experiment and theory*, *Appl. Phys. Lett.* **74** 1516 (1999)

[33] Richard M. Koehl, Satoru Adachi and Keith A. Nelson *Real-space polariton wave packet imaging*, *J. Chem. Phys.*, **110** 1317 (1999)

[34] Richard M. Koehl and Keith A. Nelson *Coherent optical control over collective vibrations traveling at lightlike speeds*, *J. Chem. Phys.*, **114** 1443 (2001)

[35] Ajay Nahata, Aniruddha S. Weling and Tony F. Heinz *A wideband coherent terahertz spectroscopy system using optical rectification and electrooptic sampling*, *Appl. Phys. Lett.*, **69** 2321 (1996)

[36] H. J. Bakker, G. C. Cho, H. Kurz, Q. Wu and X-C. Zhang, *Distortion of terahertz pulses in electro-optic sampling*, *J. Opt. Soc. Am. B* **15** 1795 (1998)

[37] G. Gallot and D. Grischkowsky *Electro-optic detection of terahertz radiation*, *J. Opt. Soc. Am. B* **16** 1204 (1999)

[38] G. N. Afanasiev, V. G. Kartavenko and J. Ruzicka *J. Phys. A: Math. Gen.*, **33** 7585 (2000)

[39] Gary P. Wiederrecht, Thomas P. Dougherty, Lisa Dhar, Keith A. Nelson, D. E. Leaird, and A. M. Weiner, *Explanation of anomalous polariton dynamics in LiTaO3*, *Phys. Rev. B*, **51** 916 (1995)

[40] C. A. Gautier, J. C. Loulergue and J. Etchepare *Homodyne and heterodyne impulsive Raman Kerr nonlinearities in crystals : application to E-symmetry polariton modes in PbTiOS*, *Solid State Commun.*, **100** 133 (1996)

[41] H. J. Bakker, S. Hunsche and H. Kurz *Coherent phonon polaritons as probes of anharmonic phonons in ferroelectrics*, *Rev. Mod. Phys.*, **70** 523 (1998)

[42] J. Hebling *Determination of the momentum of impulsively generated phonon polaritons*, *Phys. Rev.* **B 65** 092301 (2002)

[43] G. M. Gale, F. Vallee and C. Flytzanis *Propagation and Dephasing of Picosecond Phonon Polariton Pulses in Ammonium Chloride*, *Phys. Rev. Lett.* **57** 1867 (1986)

[44] V. L. Ginzburg *Radiation by uniformly moving sources*, *Physics-Uspekhi*, **39** 973 (1996)

About the Authors

R. MERLIN was born in Buenos Aires, Argentina. He received the Licenciado en Ciencias Físicas (M. Sc.) degree from the University of Buenos Aires and the Dr. rer. nat. (Ph. D.) degree from the University of Stuttgart, Germany for work performed at the Max-Planck-Institut FKF.

After a postdoctoral stay at the University of Illinois at Urbana-Champaign, he joined the Physics faculty of the University of Michigan in 1980. Since 2000, he has held a joint appointment in the Department of Electrical Engineering and Computer Science.

Dr. Merlin and collaborators pioneered experimental work on Fibonacci superlattices, the quantum-confined Pockels effect and squeezed phonons. Other significant contributions include the earliest light-scattering studies of interface phonons, folded acoustic modes and shallow impurities in GaAs/AlAs heterostructures, and the development of the technique of magneto-Raman scattering. His current research interests focus on the

generation and control of coherent vibrational and electronic fields using ultrafast laser pulses.

Dr. Merlin is a Fellow of the American Physical Society, the Optical Society of America and the von Humboldt Foundation. He is also a member of the Editorial Board of the Springer Series in Solid State Sciences and the journal Solid State Communications.

J. K. WAHLSTRAND was born in Iowa City, Iowa, USA, in 1977. He received the B.A. degree in physics from Carleton College in 1999 and is currently working toward the Ph.D. degree in the Applied Physics Program at the University of Michigan, Ann Arbor. His research is focused on coherent phonon dynamics and ultrafast time-resolved spectroscopy in semiconductors.